Randomly Switched Subsystem-based State Estimation for Active Distribution Networks with Unobservable Conditions

Shiyuan Gao, *Graduate Student Member*, *IEEE*, Hao Yu, *Senior Member, IEEE*,
Peng Li*, *Senior Member*, *IEEE*, Haoran Ji, *Senior Member*, *IEEE*, Jiancheng Yu,
Jinli Zhao, *Member*, *IEEE*, Guanyu Song, *Senior Member*, *IEEE*, and Jianzhong Wu, *Fellow, IEEE*

***Abstract*—With the high penetration of distributed generators (DGs), state estimation is essential for fast and accurate operational status tracking of active distribution networks (ADNs). However, there are generally unobservable areas in ADNs in ADNs due to the paucity of measurements. Traditional state estimation methods may encounter difficulty coping with limited measurements. Thus, aiming at the accurate and fast state perception of unobservable ADNs, this paper proposes a randomly switched subsystem-based state estimation method. First, the unobservable ADN is modeled as the randomly switched ADN (RSADN). Stochastic observability is defined to distinguish the unobservable conditions, which ensures the feasibility of state estimation. Further, considering different operational conditions, the observability enhancement mechanism is designed under limited measurement conditions to make the network observable and reduce the impact of topology switching on the system. Then, the improved unscented Kalman filter algorithm is utilized to solve the state estimation problem based on state transformation. The results of case studies confirm that the proposed method can achieve more accurate estimation results compared to other methods under unobservable conditions and exhibit satisfactory computational speed in large-scale systems.**

***Index Terms*—unobservable active distribution networks, state estimation, randomly switched active distribution networks, stochastic observability.**

NOMENCLATURE

Sets

$\mathcal{N}$	Set of all nodes
$\mathcal{L}$	Set of all lines
Θ	Set of all switching process
T_{hist}	Set of historical operational data
$\mathcal{U}_i$	Set of nodal measurements
$\mathcal{U}_{ij}$	Set of line measurements

Indices

i, j	Index of nodes
t	Index of time periods
l	Index of switching process

Variables

$\boldsymbol{x}_t$	State variables of the RSADN at time t
$\boldsymbol{y}_t$	Multi-source measurements at time t
$\boldsymbol{x}_k^+, \boldsymbol{x}_k^-$	Prior and posterior estimates for state variables of k-th subsystem
$\boldsymbol{g}_t$	System operational status change vector at time t
$\boldsymbol{A}$	System state transition matrix
$\boldsymbol{H}$	Measurement state matrix
κ	Randomly switching process
$\boldsymbol{\omega}_t, \boldsymbol{\nu}_t$	Gaussian white noises
$\boldsymbol{W}_k$	Observability matrix of k-th subsystem
$\boldsymbol{W}_\Theta$	Combined matrix for the set Θ
V_i, θ_i	Measurement of nodal voltage amplitude and phase angle
P_i, Q_i	Measurement of nodal active and reactive power injection
P_{ij}, Q_{ij}	Measurement of line active and reactive power
I_{ij}, θ_{ij}	Measurement of line current amplitude and phase angle
$\boldsymbol{M}_k$	Measurement matrix of k-th subsystem
$\boldsymbol{\mathcal{A}}_k$	Correlation matrix of k-th subsystem
ς	Measurement dispersion
$\boldsymbol{T}_k$	State transformation matrix of k-th subsystem
$\boldsymbol{z}_k$	State variables after transformation
$\boldsymbol{P}_k$	Error covariance matrix of k-th subsystem
$\boldsymbol{Q}_k$	Predicted covariance matrix of k-th subsystem

Parameters

N	Number of all nodes
N_{DG}	Number of all DGs
l	Number of switching process
$\mathscr{s}$	Number of state variables
$\mathscr{s}_k$	Number of k-th subsystem observable state variables
α_k, β_k	Smoothing parameters
$W_{\text{m}}^{(i)}, W_{\text{c}}^{(i)}$	Weights for mean and variance of Sigma point set
e	Proportional correction factor
δ	Secondary sampling factor

This work was supported by the National Natural Science Foundation of China (52277117, U24B6010), Natural Science Foundation of Tianjin (24JCYBJC01250). (*Corresponding author: Peng Li*)

S. Gao, H. Yu, P. Li, H. Ji, J. Zhao and G. Song are with the State key laboratory of Intelligent Power Distribution Equipment and System, Tianjin University, Tianjin 300072, China (email: gaosy@tju.edu.cn; tjuyh@tju.edu.cn; lip@tju.edu.cn; jihaoran@tju.edu.cn; jlzhao@tju.edu.cn; gysong@tju.edu.cn).

J. Yu is with the State Grid Tianjin Electric Power Company, Tianjin, China (email: yujiancheng@126.com).

J. Wu is with the Institute of Energy, School of Engineering, Cardiff University, Cardiff CF24 3AA, U.K. (email: wuj5@cardiff.ac.uk).

I. Introduction

With the high penetration of distributed generators (DGs), the operational status of active distribution networks (ADNs) requires enhanced precision and fast tracking [1]. The state estimation of ADNs can obtain the operational status of the entire network based on measurement data under particular parameters [2]. It is the "eye" and the basic tool for real-time monitoring, dispatching, and regulation of the ADN. Therefore, the reliability and effectiveness of state estimation are crucial for the operation of ADNs [3].

Most existing state estimation methods are based on the assumption of a sufficient measurement configuration and construct a least-squares model solved using the Gauss-Newton method. The authors in [4] proposed a fourth-order Levenberg-Marquardt approach-based Schweppe-type Huber generalized maximum-likelihood estimator to achieve statistical and numerical robustness, which demonstrated good convergence under highly stressed operating conditions. A study [5] proposed a semidefinite programming fast state estimation method based on accelerated gradient descent, which improved computational efficiency. Another study [6] proposed a second-order cone-programming-based robust state estimation method to enhance convergence and bad data identification. The authors of [7] proposed a robust state estimation method based on an exponential absolute value function to address non-Gaussian measurement noise and outliers. Although these studies have achieved significant improvements in convergence, computational speed, and robustness, the distribution network is large in scale and the measurement is difficult to fully cover, resulting in a substantial number of "blind zones" [8]. Actual distribution networks are usually unobservable network [9].

A major challenge in the state estimation of distribution networks is the unobservable condition. Insufficient measurement configuration is the main reason for the unobservable network. An unobservable ADN refers to the inability to uniquely determine the system state with countless states corresponding to the same measurement value [10]. Mathematically, when the number of measurements is less than the number of state variables, the state estimation equation is underdetermined and cannot be solved [11]. Therefore, performing state estimation under unobservable conditions is of great significance for improving the perception ability of ADNs.

Some studies utilize pseudo-measurements to achieve measurement completion [12], [13]. The authors in [14] proposed a novel maximum-likelihood state estimation method, which modeled pseudo-measurement uncertainty with any continuous distribution and greatly enhanced the flexibility of state estimation. However, pseudo-measurements generally have large measurement errors, which can affect the accuracy of state estimation [15]. Existing research on unobservable distribution network state estimation methods can be roughly divided into two categories: machine-learning and numerical methods. For the machine learning method, the authors in [16] fused supervisory control and data acquisition (SCADA)/ advanced metering infrastructure (AMI) data with pseudo-measurements based on a deep multi-fidelity Bayesian approach, which facilitated high accuracy. Another study [17] proposed a neural-network-based state estimation method to achieve high time efficiency with extended observability. However, machine-learning methods require a large amount of historical data, which may be difficult to obtain in practice. In addition, offline training may be time-consuming and lack adaptability to environmental changes.

A numerical method proposed in [18] relies on the use of allocation factors, which could deal with the underdetermined system caused by the low number of measurements. Another numerical method, matrix completion, involves supplementing missing elements of a matrix to satisfy certain constraints. Compared to machine learning methods, it only requires data from a single time instant. The authors of [19] proposed a novel matrix completion-based state estimation method with noise-resilient power flow constraints, which could effectively reduce the noise impact. Another study [20] further proposed a dynamic matrix completion-based state estimation approach that exhibited high estimation accuracy. However, owing to the utilization of optimization, the computational burden increases as the system size increases.

Recently, the randomly switched subsystem (RSS) concept proposed in [21] has been well applied in the control field. The RSS method is a very promising way to cope with unobservable conditions, which exhibits high accuracy and a relatively low computational burden. The authors of [22] applied the RSS method to continuous and discrete systems to support foundation for robust control. The RSS represents a central organizer that utilizes sequentially streamed data from subsystems, one subsystem at a time within each time interval. Motived from the concept of RSS, the topology structure can be changed by the sectionalizing and tie switches of ADNs. Thus, the ADN with different topology can be modeled as RSS. Then the state estimation with unobservable conditions can be achieved. However, the RSS method needs to be improved to adapt to the state estimation of the ADN. For one thing, irregular topology changes may deteriorate the operation of ADN. It is essential to elucidate the switching condition and path among different subsystems to reduce the impact on the ADN. Additionally, efficient solving algorithms need further research to adapt to RSS. The unscented Kalman filter (UKF) algorithm approximates the statistical properties of the state variables after nonlinear transformation through an unscented transform (UT) [23], [24], with an accuracy of at least second-order compared to the extended Kalman filter. However, UKF requires precise mastery of process and measurement noise statistical parameters, which are time-varying and difficult to accurately obtain in distribution networks. Thus, UKF needs to be improved to ensure that state estimation of RSS can be efficiently solved.

Therefore, further research is required on state estimation for unobservable ADNs in the following aspects. a) Multi-source measurements exist in the distribution network although measurements are limited. Fully utilizing multi-source measurements to improve accuracy of state estimation still needs to be addressed. b) Considering safe operation, the ADN generally does not allow frequent system switching in the short term. Thus, achieving state estimation by as few switches as possible is significant for reducing the impact on the actual ADN. c) The state equation of distribution networks is usually established by time series prediction methods. The process and measurement noise statistical parameters are difficult to obtain due to fluctuations of DGs and loads. The efficient solving algorithm needs further research.

To address these issues, this paper proposes a state estimation method for unobservable distribution networks, as shown in Fig. 1. The unobservable ADN (gray area) is modeled as a randomly switched active distribution network (RSADN) by multiple subsystems. However, irregular topology changes may deteriorate the operation of ADN. The switching path is revealed to reduce frequent switching and ensure the feasibility of state estimation. Furthermore, the high-dimensional state variables are mapped to low-dimensional transformed variables to reduce the computational burden, which also exhibits satisfactory computational speed in large-scale systems. The contributions of this study are summarized as follows:

1) A state estimation method for unobservable RSADN is proposed based on topology switching. The RSADN model is constructed to adapt to the distribution network with limited measurements. The concept of traditional observability is transformed into stochastic observability based on the combined matrix. The state estimation problem can be solved efficiently and exhibits satisfactory accuracy.

2) An observability-improving mechanism is proposed for distribution networks under limited measurements. The switching guiding criterion is designed to reveal the switching path to make the network observable and reduce the impact of topology switching on the system.

3) A measurement supplementary strategy is proposed in scenarios where the switching guidance criteria fail. The measurement configuration that satisfies network observability is supplemented based on the combined matrix, which can further guide the measurement configuration of unobservable networks.

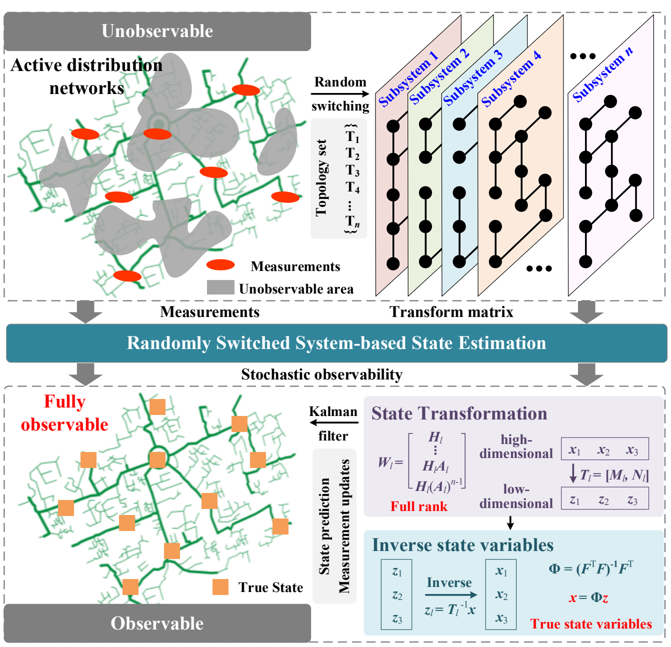

Fig. 1. Framework of proposed state estimation method.

The remainder of this paper is organized as follows. Section II introduces the modeling of randomly switched unobservable distribution networks. Section III presents the proposed method of state estimation of unobservable distribution networks based on the state-transformation method. Case studies and analyses are discussed in Section IV. Finally, the conclusions are presented in Section V.

II. Modeling of Randomly Switched Unobservable Distribution Networks

The RSADN model was established to perform state estimation on unobservable distribution networks. Stochastic observability is defined to evaluate the feasibility of the state estimation. On this basis, a switching-guiding mechanism for the RSADN under unobservable conditions is designed to reduce the number of switches.

A. Modelling of Unobservable RSADN

Consider a distribution network with nodes denoted by the set $\mathcal{N} := \{1,2,\dots,N\}$, and lines denoted by the set $\mathcal{L} := \{ij|i,j \in \mathcal{N}\}$. In general, the voltage amplitude and phase angle of all the nodes are selected as the state variables. The unobservable RSADN model for state estimation comprises the state transition process and the measurement equation, which are expressed as follows:

$$\begin{cases} \boldsymbol{x}_{t+1} = \boldsymbol{A}(\kappa(t))\boldsymbol{x}_t + \boldsymbol{g}_t + \boldsymbol{\omega}_t \\ \boldsymbol{y}_t = \boldsymbol{H}(\kappa(t))\boldsymbol{x}_t + \boldsymbol{\nu}_t \end{cases} \tag{1}$$

where $\boldsymbol{y}_t$ represents multi-source measurements, including nodal voltage, line current, nodal power injection, and line power measurements, etc. Further, $\kappa(t)$ represents the randomly switching process of the distribution network and $\boldsymbol{\omega}_t$ and $\boldsymbol{\nu}_t$ are Gaussian white noises and are independently distributed.

The system matrices $\boldsymbol{A}(\kappa(t))$ and $\boldsymbol{H}(\kappa(t))$ depend on the randomly switching process $\kappa(t)$ that takes m possible values in a discrete state space $\Theta = \{1,2,\dots,m\}$. For each $m \in \Theta$, the corresponding matrix $\boldsymbol{A}(\kappa(i))$ and $\boldsymbol{H}(\kappa(i))$ form the m-th subsystem of the unobservable RSADN. The discrete switching process $\kappa(t)$ is a piecewise constant that takes values in a finite set and satisfies the following assumptions.

Assumption 1: For a given period, 1) the discrete switching process $\kappa(t)$ can only occur at the measurement time $k\delta, k = 1,2,\dots$, which means $\kappa(t) = \kappa(k\delta)$; 2) $\kappa(k\delta)$ is independent and identically distributed (i.i.d), satisfying (2):

$$P(\kappa(k\delta) = i) = p_i > 0, i \in \Theta, \text{ and } \textstyle\sum_{i=1}^{m} p_i = 1 \tag{2}$$

Assumption 1 ensures the independence and uniqueness of switching with only one operational mode at each time interval, which means only one subsystem at each time interval.

For a sequence $\kappa(k\delta), k = 1,2,\dots,l$, define the stochastic matrix sequences $\boldsymbol{A}_k = \boldsymbol{A}(\kappa(k\delta))$, $\boldsymbol{H}_k = \boldsymbol{H}(\kappa(k\delta))$. Under Assumption 1, the following equations hold.

$$\boldsymbol{A}_k = \textstyle\sum_{i=1}^{m} \boldsymbol{A}(\kappa(i))\boldsymbol{1}, \boldsymbol{H}_k = \sum_{i=1}^{m} \boldsymbol{H}(\kappa(i))\boldsymbol{1} \tag{3}$$

where $\boldsymbol{1}$ is the identity matrix. These matrices are random.

The state estimation model (1) is a linear model. Although distribution networks are complex, and their topologies and power loads may change frequently, linearization can still ensure high accuracy in specific scenarios. Holt's two-parameter exponential smoothing method is a widely used method for obtaining enough accurate models [25]. It uses recursive algorithms to calculate the state transition matrix at each instant. Therefore, the models become closer to the actual nonlinear models as the algorithm progresses.

Thus, it is adopted to model the state transition process of the unobservable RSADN, which is described as follows:

$$\boldsymbol{A}_k = \alpha_k(1+\beta_k)\mathbf{I}, 0 \le \alpha_k, \beta_k \le 1 \tag{4a}$$

$$\boldsymbol{g}_k = (1+\beta_k)(1-\alpha_k)\boldsymbol{x}_k - \beta_k\boldsymbol{\lambda}_k + (1-\beta_k)\boldsymbol{\xi}_k \tag{4b}$$

$$\boldsymbol{\lambda}_k = \alpha_k\boldsymbol{x}_k^+ + (1-\alpha_k)\boldsymbol{x}_k^- \tag{4c}$$

$$\boldsymbol{\xi}_k = \beta_k(\boldsymbol{\lambda}_k - \boldsymbol{\lambda}_{k-1}) + (1-\beta_k)\boldsymbol{\xi}_{k-1} \tag{4d}$$

where $\boldsymbol{g}_k$ is the system operational status change vector. α_k and β_k are the Holt's two parameters. $\boldsymbol{\lambda}_k$ and $\boldsymbol{\xi}_k$ are the auxiliary variables.

For measurement state matrix $\boldsymbol{H}$, Taylor expansion is utilized to realize linearization. And $\boldsymbol{H}$ is topologically related, which needs recalculation when topology changes.

B. Stochastic Observability on Finite-time Interval

Observability is a prerequisite for state estimation. For an unobservable RSADN, stochastic observability is defined instead of traditional observability state estimation, which is an extension of the classical binary observability. For the k-th subsystem of sequence $\{1,2,\dots,l\}$, the observability matrix is defined as follows:

$$\boldsymbol{W}_k = \begin{bmatrix} H_k \\ H_kA_k \\ \vdots \\ H_k(A_k)^{\mathscr{s}-1} \end{bmatrix}, k = 1,\dots,l \tag{5}$$

where $\mathscr{s}$ is the number of state variables.

The combined matrix for the set Θ is:

$$\boldsymbol{W}_\Theta = \begin{bmatrix} W_1 \\ W_2 \\ \vdots \\ W_k \end{bmatrix} \tag{6}$$

Both $\boldsymbol{W}_k$ and $\boldsymbol{W}_\Theta$ are constant matrices. No randomness is involved. The randomness originates from the switching sequence $\kappa(k\delta)$ during system operation, such as line switching and supply restoration.

Assumption 2: For any subsystem $k \in \Theta$, 1) the subsystem is unobservable, namely, $\text{rank}(\boldsymbol{W}_k) = \mathscr{s}_k < \mathscr{s}$; 2) $\boldsymbol{W}_\Theta$ is full column rank.

Remark: Condition 1) in Assumption 2 indicates that all subsystems are unobservable, including the extreme cases $\mathscr{s}_k = 0$, which represent the total loss of the sensing capability. Condition 2) in Assumption 2 ensures that collective observable subspaces cover all spaces. In other words, if $\boldsymbol{W}_\Theta$ is not full column rank, all subsystems cannot be observed. Thus, define stochastic observability as follows:

Stochastic observability: if the combined matrix $\boldsymbol{W}_\Theta$ is full column rank, stochastic observability is achieved in a finite-time interval with a positive probability for the unobservable RSADN. Stochastic observability is an extension of the classical binary "observability" to probabilistic "stochastic observability." Similarly, for the observer design, feedback-based linear observer structures are utilized for the subsystems in the next section.

C. Subsystem Switching Guidance

For an unknown RSADN, satisfaction with stochastic observability is crucial for state estimation. In this section, a subsystem switching guidance mechanism is designed to reveal the switching path of the unobservable RSADN. Specifically, the following two situations (observable and unobservable conditions) are discussed:

1) Historical data satisfies stochastic observability

Owing to maintenance or switching operations on distribution lines, the historical operational data includes the topology structure of the subsystem and corresponding measurements, represented by $T_{\text{hist}} = \{T_1, T_2, \dots T_\chi\}$. If these data satisfy the stochastic observability requirements after calculation according to (5) and (6), the system need not actively switch topologies and can directly perform state estimation.

Note that this condition means that the measurements obtained at each previous time interval did not satisfy observability, but all data of T_{hist} satisfies stochastic observability.

2) Historical data does not satisfy stochastic observability

If the historical data still cannot satisfy the requirements of stochastic observability, the system must perform a finite number of topology switches. Therefore, the concept of measurement dispersion, which essentially determines the degree of measurement, is defined. The more scattered the measurements, the more abundant and available information will be provided. The expected topological changes should increase the measurement dispersion, thereby guiding the changes in the topological structure. Specifically, measurement dispersion is calculated as follows:

(a) Reorganize the measurements. For the nodal measurements, the measurement group comprised the following:

$$\mathcal{U}_i = [V_i, \theta_i, P_i, Q_i] \tag{7}$$

For line measurement, the measurement group involves:

$$\mathcal{U}_{ij} = [P_{ij}, Q_{ij}, I_{ij}, \theta_{ij}] \tag{8}$$

(b) Define the measurement matrix $\boldsymbol{M} = \{\boldsymbol{M}_1, \boldsymbol{M}_2, \dots, \boldsymbol{M}_k\}$. For $\boldsymbol{M}_k$, each row and column represent a node label, and the corresponding element represents the number of measurements. The primary diagonal elements represent the number of nodal measurements, whereas the remaining positions represent the number of line measurements. For example, $\boldsymbol{M}_k(2,2) = 3$ indicates that three nodal measurements exist for node 2. $\boldsymbol{M}_k(2,3) = 2$ indicates that there are two measurements in line 23. Therefore, the total number of measurements of subsystem k is the sum of the elements of measurement matrix $\boldsymbol{M}_k$.

(c) Calculate the correlation matrix $\boldsymbol{\mathcal{A}}_k$ of the subsystem k based on the definition of the correlation matrix in an undirected graph.

(d) Calculate the measurement dispersion of subsystem k based on the measurement matrix $\boldsymbol{M}_k$ and correlation matrix $\boldsymbol{\mathcal{A}}_k$, as follows:

$$\rho_\mu = \frac{\sum_{\eta=1}^{N} \boldsymbol{M}_k(\mu,\eta)}{\sum_{\eta=1}^{N} \boldsymbol{\mathcal{A}}_k(\mu,\eta)+1}, \mu = 1,2, \dots N \tag{9a}$$

$$\varsigma = \mathrm{var}[\rho_1, \dots, \rho_\mu, , \dots, \rho_N], \mu = 1,2, \dots N \tag{9b}$$

where ρ_μ represents the proportion of measurements related to node μ in the current subsystem k; ς represents the measurement dispersion; $\mathrm{var}[*]$ represents the variance.

In summary, the evolution rule of the switching path is as follows: After switching, the measurement dispersion ς should not be less than before, and the maximum number of switching is $\varrho = \mathscr{s} - \mathrm{rank}(\boldsymbol{W}_\Theta)$.

3) Measurement supplementary strategy

In some cases, due to limited measurement configurations, stochastic observability may still not be satisfied after the maximum number of switching ϱ. More measurements are required to be configured. The measurement supplementary strategy is given as follows:

(a) Establish observability matrices $\{\boldsymbol{W}_s, \dots, \boldsymbol{W}_{s+\varrho}\}$ for the ϱ topologies according to the switching guidance criteria.

(b) Construct the combined matrix $\boldsymbol{W}_\Theta$ using $\{\boldsymbol{W}_1, \dots, \boldsymbol{W}_k\}$ and $\{\boldsymbol{W}_s, \dots, \boldsymbol{W}_{s+\varrho}\}$.

(c) Calculate the maximum linearly independent group of $\boldsymbol{W}_\Theta$. Supplement power or voltage measurements at relevant nodes until the rank of the maximum linearly independent group is equal to $\mathscr{s}$.

Remark: The stochastic observability can be achieved by the switching guiding mechanism with as few switches as possible. Although the proposed method also provides an observability-improving mechanism under limited measurement conditions, the supplementary measurements may not meet the optimal economic requirements. The aim is to enhance the observability of the distribution network by minimizing network switching and adding as few new measurements as possible.

The following example is given to clearly illustrate the measurement dispersion.

Example: Consider the topology structure shown in Fig. 2 (topology 1); the measurement configuration is presented in Table 1.

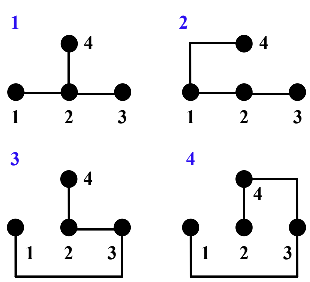

Fig. 2. Diagram of topology switching.

TABLE I

MEASUREMENT CONFIGURATION OF TOPOLOGY 1

Measurement type		Number of measurements	Number of state variables
Nodal measurement	Line measurement		
$\begin{bmatrix} V_1 \\ P_2, Q_2 \\ 0 \\ 0 \end{bmatrix}$	$\begin{bmatrix} 0 \\ P_{23}, Q_{23}, I_{24} \\ 0 \\ 0 \end{bmatrix}$	6	7

Under Topology 1, the measurement matrix $\boldsymbol{M}_1$ and correlation matrix $\boldsymbol{\mathcal{A}}_1$ can be organized as follows:

$$\boldsymbol{M}_1 = \begin{bmatrix} 1 & 0 & 0 & 0 \\ 0 & 2 & 2 & 1 \\ 0 & 2 & 0 & 0 \\ 0 & 1 & 0 & 0 \end{bmatrix}, \boldsymbol{\mathcal{A}}_1 = \begin{bmatrix} 0 & 1 & 0 & 0 \\ 1 & 0 & 1 & 1 \\ 0 & 1 & 0 & 0 \\ 0 & 1 & 0 & 0 \end{bmatrix} \tag{10}$$

The rank of the observability matrix is $\mathrm{rank}(\boldsymbol{W}_1) = 6 < 7$. Thus, the current system is unobservable with a maximum number of switching $7 - 6 = 1$. According to (9), the measurement dispersion ς_1 is 0.1406. Then, the topology with the highest measurement dispersion is selected from all candidate topology sets for switching. Assume that there are three candidate topologies, as shown in Fig. 2 (topologies 2, 3, and 4):

The measurement matrix and correlation matrix can be organized separately as follows:

$$\boldsymbol{M}_2 = \begin{bmatrix} 1 & 0 & 0 & 0 \\ 0 & 2 & 2 & 0 \\ 0 & 2 & 0 & 0 \\ 0 & 0 & 0 & 0 \end{bmatrix}, \boldsymbol{\mathcal{A}}_2 = \begin{bmatrix} 0 & 1 & 0 & 1 \\ 1 & 0 & 1 & 0 \\ 0 & 1 & 0 & 0 \\ 1 & 0 & 0 & 0 \end{bmatrix} \tag{11a}$$

$$\boldsymbol{M}_3 = \begin{bmatrix} 1 & 0 & 0 & 0 \\ 0 & 2 & 2 & 1 \\ 0 & 2 & 0 & 0 \\ 0 & 1 & 0 & 0 \end{bmatrix}, \boldsymbol{\mathcal{A}}_3 = \begin{bmatrix} 0 & 0 & 1 & 0 \\ 0 & 0 & 1 & 1 \\ 1 & 1 & 0 & 0 \\ 0 & 1 & 0 & 0 \end{bmatrix} \tag{11b}$$

$$\boldsymbol{M}_4 = \begin{bmatrix} 1 & 0 & 0 & 0 \\ 0 & 2 & 0 & 1 \\ 0 & 0 & 0 & 0 \\ 0 & 1 & 0 & 0 \end{bmatrix}, \boldsymbol{\mathcal{A}}_4 = \begin{bmatrix} 0 & 0 & 1 & 0 \\ 0 & 0 & 0 & 1 \\ 1 & 0 & 0 & 1 \\ 0 & 1 & 1 & 0 \end{bmatrix} \tag{11c}$$

The measurement dispersion can be calculated, where $\varsigma_2 = 0.3704$, $\varsigma_3 = 0.3148$, $\varsigma_4 = 0.5$. Therefore, topology 4 is selected as the switching path. After switching, the rank of the combined matrix is 7, satisfying the stochastic observability condition. The calculation process of the combined matrix can be found in the Appendix.D.

III. STATE ESTIMATION OF UNOBSERVABLE RSADN BASED ON STATE TRANSFORMATION

In this section, the state estimation algorithm is designed for the subsystem observers. The state of each subsystem will be organized into an observer for the entire state. An improved UKF approach is applied to solver the state estimation problem. The design step is simple and constructive to ensure the accuracy and computational speed.

A. Transformation of State Variables

Let $\boldsymbol{W}_k$ be the observability matrix of the k-th subsystem defined in (5). Because each subsystem is unobservable, $\mathrm{rank}(\boldsymbol{W}_k) = \mathscr{s}_i < \mathscr{s}$. The base vector $\boldsymbol{Y}_k$ matrix is defined as follows:

$$\boldsymbol{Y}_k = \mathrm{Base}(\ker(\boldsymbol{W}_k)) \in \mathbb{R}^{\mathscr{s} \times (\mathscr{s} - \mathscr{s}_k)} \tag{12}$$

where ker $(*)$ is the kernel or null space, $\ker(\boldsymbol{W}_k) = \{\varepsilon \in \mathbb{R}^{s-s_k} | \boldsymbol{W}_k \varepsilon = 0\}$; Base$(*)$ is to take the base vector in the space $*$.

Select any matrix $\boldsymbol{Z}_k \in \mathbb{R}^{s \times s_k}$ to form the state transformation matrix $\boldsymbol{T}_k$, and make $\boldsymbol{T}_k$ invertible:

$$\boldsymbol{T}_k = [\boldsymbol{Y}_k, \boldsymbol{Z}_k] \tag{13}$$

The inverse of $\boldsymbol{T}_k$ is decomposed into:

$$\boldsymbol{T}_k^{-1} = \begin{bmatrix} \boldsymbol{G}_k \\ \boldsymbol{F}_k \end{bmatrix}, \boldsymbol{G}_k \in \mathbb{R}^{(s-s_k) \times s}, \boldsymbol{F}_k \in \mathbb{R}^{s_k \times s} \tag{14a}$$

$$\boldsymbol{F} = \begin{bmatrix} \boldsymbol{F}_1 \\ \boldsymbol{F}_2 \\ \vdots \\ \boldsymbol{F}_k \end{bmatrix} \in \mathbb{R}^{s_\Theta \times s}, s_\Theta = \sum_{i=1}^{k} s_i \tag{14b}$$

Lemma 1: 1) $\ker(\boldsymbol{F}_k) = \ker(W_k)$; 2) $\ker(\boldsymbol{F}) = \ker(\boldsymbol{W}_\Theta)$. The detailed proof is provided in Appendix A.

The state transformation $\tilde{\boldsymbol{z}}_k = \boldsymbol{T}_k^{-1}\boldsymbol{x}$ can be decomposed into:

$$\tilde{\boldsymbol{z}}_k = \boldsymbol{T}_k^{-1}\boldsymbol{x} = \begin{bmatrix} \boldsymbol{G}_k\boldsymbol{x} \\ \boldsymbol{F}_k\boldsymbol{x} \end{bmatrix} = \begin{bmatrix} \boldsymbol{v}_k \\ \boldsymbol{z}_k \end{bmatrix} \tag{15}$$

After this transformation, the system state transition matrix $\boldsymbol{A}_k$ and measurement matrix $\boldsymbol{H}_k$ can be converted to

$$\widetilde{\boldsymbol{A}}_k = \boldsymbol{T}_k^{-1}\boldsymbol{A}_k\boldsymbol{T}_k, \widetilde{\boldsymbol{H}}_k = \boldsymbol{H}_k\boldsymbol{T}_l \tag{16}$$

and $\widetilde{\boldsymbol{A}}_k$ and $\widetilde{\boldsymbol{H}}_k$ have the following structures:

$$\begin{gathered} \widetilde{\boldsymbol{A}}_k = \begin{bmatrix} \widetilde{\boldsymbol{A}}_k^{11} & \widetilde{\boldsymbol{A}}_k^{11} \\ 0 & \widetilde{\boldsymbol{A}}_k^{22} \end{bmatrix}, \widetilde{\boldsymbol{A}}_k^{22} \in \mathbb{R}^{s_k \times s_k} \\ \widetilde{\boldsymbol{H}}_k = \left[0, \widetilde{\boldsymbol{H}}_k^2\right], \widetilde{\boldsymbol{H}}_k^2 \in \mathbb{R}^{1 \times s_k} \end{gathered} \tag{17}$$

Thus, only the transformed state variable $\boldsymbol{z}_k$ needs to be focused on, and the system model (1) can be transformed into (18).

$$\begin{cases} \boldsymbol{z}_{k+1} = \widetilde{\boldsymbol{A}}_k^{22}\boldsymbol{z}_k \\ \boldsymbol{y}_k = \widetilde{\boldsymbol{H}}_k^2\boldsymbol{z}_k \end{cases} \tag{18}$$

and $\widetilde{\boldsymbol{A}}_k^{22}$, $\widetilde{\boldsymbol{H}}_k^2$ is observable. The observer for the k-th subsystem will estimate $\boldsymbol{z}_k$ only.

Define the true value, estimated value, and estimated error as follows:

$$\boldsymbol{z} = \begin{bmatrix} \boldsymbol{z}_1 \\ \boldsymbol{z}_2 \\ \vdots \\ \boldsymbol{z}_k \end{bmatrix} \in \mathbb{R}^{s_\Theta}, \hat{\boldsymbol{z}} = \begin{bmatrix} \hat{\boldsymbol{z}}_1 \\ \hat{\boldsymbol{z}}_2 \\ \vdots \\ \hat{\boldsymbol{z}}_k \end{bmatrix} \in \mathbb{R}^{s_\Theta} \tag{19a}$$

$$\boldsymbol{e}_k = \boldsymbol{z}_k - \hat{\boldsymbol{z}}_k, \boldsymbol{e} = \boldsymbol{z} - \hat{\boldsymbol{z}} \tag{19b}$$

$$\boldsymbol{\mu}_k = ||\boldsymbol{e}_k||, \boldsymbol{\mu} = ||\boldsymbol{e}|| \tag{19c}$$

B. State Estimation Method Based on Improved UKF

1) State estimation based on UKF

The improved UKF is utilized to solve (18). First, the sigma point set is constructed using the UT. Owing to the high dimensionality of the state variables in the unobservable RSADN, this paper chooses the symmetric proportional correction sampling method to ensure the accuracy and numerical stability of the algorithm.

For subsystem k, select $2s_k + 1$ sets of sigma points with the same mean and variance as the state vector. The sigma point set and its weights are shown as follows:

$$\boldsymbol{\chi}_i^- = \begin{cases} \bar{\boldsymbol{z}}_k & i = 0 \\ \bar{\boldsymbol{z}}_k + \left(\sqrt{(s_k + \varphi)\boldsymbol{P}_k}\right)_i & i = 1, \dots, s_k \\ \bar{\boldsymbol{z}}_k - \left(\sqrt{(s_k + \varphi)\boldsymbol{P}_k}\right)_i & i = s_k + 1, \dots, 2s_k \end{cases} \tag{20a}$$

$$W_{\mathrm{m}}^{(i)} = \begin{cases} \frac{\varphi}{s_k + \varphi} & i = 0 \\ \frac{1}{2(s_k + \varphi)} & i = 1, \dots, 2s_k \end{cases} \tag{20b}$$

$$W_{\mathrm{c}}^{(i)} = \begin{cases} \frac{\varphi}{s_k + \varphi} + 1 - e^2 + \xi & i = 0 \\ \frac{1}{2(s_k + \varphi)} & i = 1, \dots, 2s_k \end{cases} \tag{20c}$$

where $\boldsymbol{\chi}_i^-$ is the i-th sigma point constructed; the tuning parameter $\varphi = e^2(s_k + \delta) - s_k$ is used to control the distance from the point to the mean. Further, e is the proportional correction factor, with the commonly used values being $10^{-4} \le e \le 1$ for Gaussian distributions; δ is the secondary sampling factor, usually set as 0 or $3 - s_k$; and ξ is the candidate parameter, and adjusting ξ can improve the accuracy of variance approximation. In addition, $\left(\sqrt{(s_k + \varphi)\boldsymbol{P}_k}\right)_i$ represents the i-th column; $W_{\mathrm{m}}^{(i)}$ and $W_{\mathrm{c}}^{(i)}$ are weights for mean and variance respectively.

Substitute each set of sigma points into (18) for propagation. The mean and covariance of the propagated sigma point set are calculated as follows:

$$\tilde{\boldsymbol{z}}_{k+1} = \widetilde{\boldsymbol{A}}_k^{22}\boldsymbol{\chi}_i^- \tag{21a}$$

$$\bar{\boldsymbol{z}}_{k+1} = \sum W_{\mathrm{m}}(i)\tilde{\boldsymbol{z}}_{k+1} \tag{21b}$$

$$\widetilde{\boldsymbol{P}}_k = \sum W_{\mathrm{c}}(i)(\tilde{\boldsymbol{z}}_{k+1} - \bar{\boldsymbol{z}}_{k+1})(\tilde{\boldsymbol{z}}_{k+1} - \bar{\boldsymbol{z}}_{k+1})^{\mathrm{T}} + \boldsymbol{Q}_k \tag{21c}$$

Based on the predicted values, the UT is performed again according to (20) to obtain a new sigma point set. Substitute the new sigma point into (18) to obtain the measurement prediction values. Calculate the measurement prediction mean and covariance matrix, which are shown as follows:

$$\boldsymbol{\chi}_i^+ = \begin{cases} \bar{\boldsymbol{z}}_{k+1} & i = 0 \\ \bar{\boldsymbol{z}}_{k+1} + \left(\sqrt{(s_k + \varphi)\widetilde{\boldsymbol{P}}_k}\right)_i & i = 1, \dots, s_k \\ \bar{\boldsymbol{z}}_{k+1} - \left(\sqrt{(s_k + \varphi)\widetilde{\boldsymbol{P}}_k}\right)_i & i = s_k + 1, \dots, 2s_k \end{cases} \tag{22a}$$

$$\tilde{\boldsymbol{y}}_{k+1} = \widetilde{\boldsymbol{H}}_k^2\boldsymbol{\chi}_i^+ \tag{22b}$$

$$\bar{\boldsymbol{y}}_{k+1} = \sum W_{\mathrm{m}}^{(i)}\tilde{\boldsymbol{y}}_{k+1} \tag{22c}$$

$$\widetilde{\boldsymbol{P}}_{yy,k} = \sum W_{\mathrm{c}}^{(i)}(\tilde{\boldsymbol{y}}_{k+1} - \bar{\boldsymbol{y}}_{k+1})(\tilde{\boldsymbol{y}}_{k+1} - \bar{\boldsymbol{y}}_{k+1})^{\mathrm{T}} + \boldsymbol{R}_k \tag{22d}$$

$$\widetilde{\boldsymbol{P}}_{zy,k} = \sum W_{\mathrm{c}}^{(i)}(\tilde{\boldsymbol{z}}_{k+1} - \bar{\boldsymbol{z}}_{k+1})(\tilde{\boldsymbol{y}}_{k+1} - \bar{\boldsymbol{y}}_{k+1})^{\mathrm{T}} \tag{22e}$$

where $\widetilde{\boldsymbol{P}}_{yy,k}$, $\widetilde{\boldsymbol{P}}_{zy,k}$ are the covariance and cross-covariance matrices of the predicted measurements, respectively.

Then calculate the Kalman gain, and the state vector and covariance matrix are updated to obtain the state estimation result, which is illustrated as follows:

$$\boldsymbol{K}_{k+1} = \widetilde{\boldsymbol{P}}_{zy,k}\left(\widetilde{\boldsymbol{P}}_{yy,k}\right)^{-1} \tag{23a}$$

$$\hat{\boldsymbol{z}}_{k+1} = \tilde{\boldsymbol{z}}_{k+1} + \boldsymbol{K}_{k+1}(\boldsymbol{y}_{k+1} - \tilde{\boldsymbol{y}}_{k+1}) \tag{23b}$$

$$\widehat{\boldsymbol{P}}_{k+1} = \widehat{\boldsymbol{P}}_k - \boldsymbol{K}_{k+1}\widetilde{\boldsymbol{P}}_{yy,k}\boldsymbol{K}_{k+1}^{\mathrm{T}} \tag{23c}$$

Finally, invert the transformed state variable $\hat{\boldsymbol{z}}_{k+1}$ to $\widehat{\boldsymbol{x}}_{k+1}$:

$$\hat{\boldsymbol{z}}_{k+1} = \boldsymbol{F}_k\widehat{\boldsymbol{x}}_k = \boldsymbol{F}_k\boldsymbol{A}_k\widehat{\boldsymbol{x}}_k = \boldsymbol{F}_k\boldsymbol{A}_k\boldsymbol{\Phi}\hat{\boldsymbol{z}}_{k+1} \tag{24a}$$

$$\boldsymbol{\Phi} = (\boldsymbol{F}'\boldsymbol{F})^{-1}\boldsymbol{F} \tag{24b}$$

$$\boldsymbol{x}_{k+1} = \boldsymbol{\Phi}\hat{\boldsymbol{z}}_{k+1} \tag{24c}$$

2) Improved fault-tolerant noise statistical estimator

To reduce the impact of the process noise on the accuracy, a new noise statistic estimator is introduced to ensure robustness while retaining most of the covariance correction terms. The improved fault-tolerant noise statistical estimator comprised an unbiased noise statistical estimator and biased noise statistical estimator, which is described as follows:

$$\begin{aligned}\boldsymbol{Q}_{k+1} &= (1-d_k)\boldsymbol{Q}_k + \\ &d_k[\mathrm{diag}(\hat{\boldsymbol{z}}_k - \bar{\boldsymbol{z}}_k)^2 - (\widehat{\boldsymbol{P}}_k - \widetilde{\boldsymbol{P}}_k + \boldsymbol{Q}_k)]\end{aligned} \tag{25a}$$

$$d_k = \frac{1-b}{1-b^{k+1}} \tag{25b}$$

where d_k is the comprehensive forgetting factor, b is a constant which is set to be 0.96.

The subtraction in (25) may still cause the estimated noise covariance matrix to lose semi-positive definiteness. Therefore, (25) is further transformed into (26), which is a biased estimate.

$$\begin{aligned}\boldsymbol{Q}_{k+1} &= (1-d_k)\boldsymbol{Q}_k + \\ &d_k[\mathrm{diag}(\hat{\boldsymbol{z}}_k - \bar{\boldsymbol{z}}_k)^2 + \boldsymbol{K}_k\widetilde{\boldsymbol{P}}_{yy,k}\boldsymbol{K}_k^{\mathrm{T}}]\end{aligned} \tag{26}$$

In summary, an improved fault-tolerant statistical noise estimator is obtained by combining a biased noise statistical estimator with an unbiased noise statistical estimator.

C. Implementation of State Estimation

The flowchart of the proposed state-estimation method is shown in Fig. 3.Firstly, check whether the historical operational data meet the requirements of stochastic observability. By calculating the measurement dispersion, select the switching path of the unobservable RSADN to reduce frequent topological switching. Subsequently, the transformation matrix is constructed, and state estimation is performed based on the improved UKF.

Remark: For scenarios with sufficient measurements, if measurement interruption leads to unobservability, the proposed method can still demonstrate effective adaptability. However, if there are inadequate measurements, the stochastic observability may remain unsatisfactory, even after several switches. Therefore, the proposed method is not applicable. Additional measurements must be configured for the RSADN.

In summary, the proposed method based on RSSs can effectively solve the operational state of the unobservable RSADN. It can conduct accurate state estimation under unobservable conditions and ensure computational speed.

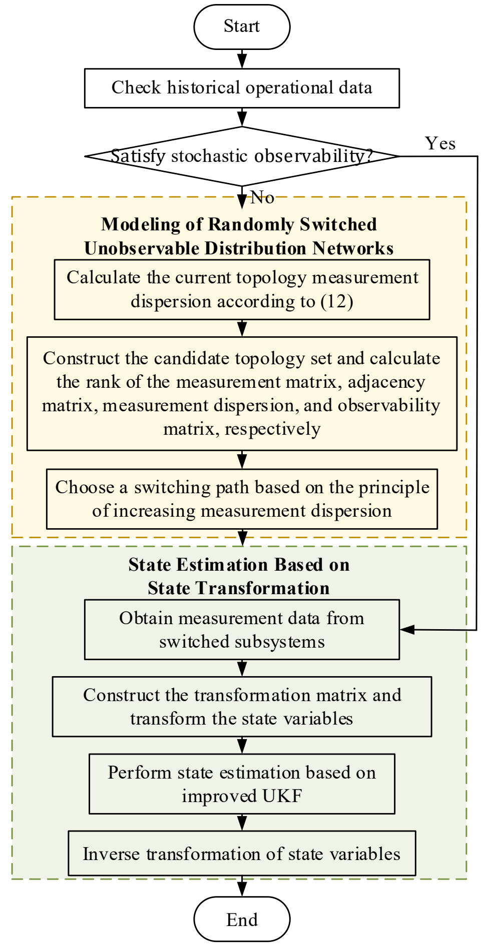

Fig. 3. Flowchart of state estimation method.

IV. Case Studies and Analysis

In this section, the effectiveness of the proposed state estimation method is verified using modified IEEE 33-node and IEEE 123-node networks. The proposed method is implemented with MATLAB R2020a. All numerical experiments are carried out on an Intel Core i7 @ 3.20GHz computer with 16GB RAM.

A. Analysis of Measurement Configuration

The topology of the modified IEEE 33-node distribution network is shown in Fig. 4. The system consists of 32 lines with a rated voltage level of 12.66 kV. The total active and reactive power demands are 3715.0 kW and 2300.0 kVAr, respectively. To consider the impact of the high penetration of DGs, six photovoltaics (PVs) and seven wind turbines (WTs) are integrated into the system, whose active power reaches approximately 100% of the peak demand. The DG capacity parameters are listed in Table II. The daily DGs and loads operation curves are shown in Appendix Fig. B.

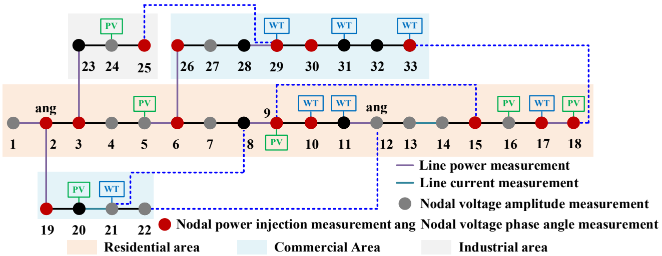

Fig. 4. Structure of modified IEEE 33-node distribution network.

TABLE II

PARAMETER OF DG INVERTER

Location	Type	Capacity (kVA)	Location	Type	Capacity (kVA)
5	PV	100	10	WT	100
9	PV	100	11	WT	200
16	PV	300	21	WT	200
18	PV	300	29	WT	200
20	PV	300	17	WT	500
24	PV	300	31	WT	500
			33	WT	500

To verify the effectiveness of the proposed method, the following four schemes are considered.

Scheme I: The true value of operational state is obtained from OpenDSS.

Scheme II: The traditional Gauss-Newton method is utilized to solve the state estimation.

Scheme III: The proposed method is utilized to solve the state estimation.

Scheme IV: The matrix completion method in [19] is utilized to solve the state estimation (seen in Appendix B).

Scheme V: The pseudo-measurement-based method in [14] is utilized to solve the state estimation.

The true value is simulated using OpenDSS [26], and the measurement value is generated by adding random measurement noise of the Gaussian distribution to the real value. For simplification, the measurement noise standard deviations of AMI, SCADA, and distribution phasor measurement unit (D-PMU) are 5%, 1%, and 0.1%, respectively.

The solutions for the estimation accuracy in Schemes II, III, and IV are compared. The mean absolute percentage error (MAPE) is selected to estimation accuracy analysis.

$$\text{Mean Absolute Percentage Error (MAPE)} = \frac{1}{N}\sum_{i=1}^{N}\left|\frac{V_{i,\text{se}}-V_{i,\text{true}}}{V_{i,\text{true}}}\right| + \frac{1}{N-1}\sum_{i=2}^{N}\left|\frac{\theta_{i,\text{se}}-\theta_{i,\text{true}}}{\theta_{i,\text{true}}}\right| \tag{27}$$

The relationship between the measurement redundancy and MAPE is shown in Fig. 5. When the measurement redundancy exceeds 1 (observable condition), the estimation accuracies of Schemes II, III, and V are at the same level, and both are superior to those of Scheme IV. When the measurement redundancy is less than 1, Scheme II is no longer applicable, and Scheme III is optimal. Thus, the proposed method can ensure a high accuracy of state estimation, even with unobservable networks, which can effectively improve the perception ability of the distribution network.

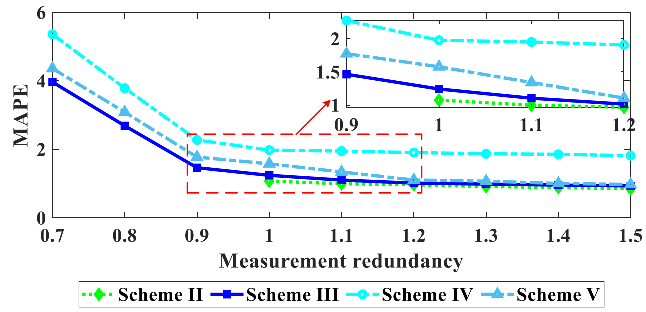

Fig. 5. Relationship between measurement redundancy and MAPE.

B. Analysis of Unobservable Conditions

Table III lists the number of measurements and state variables. Currently, the rank of the combined matrix is 57, which is less than 65. Thus, the current measurement configuration is not observable.

According to Assumption 3, the network must perform a finite number of active switches to satisfy the stochastic observability. The measurement dispersion can be calculated to be 0.3429 based on (9). The proposed switching-guiding mechanism is utilized to select the switching path, as listed in Table IV. The direction with the highest measurement dispersion is selected for each switch. After three network switches, the combined matrix reaches full column rank, satisfying the requirement for stochastic observability.

To verify the effectiveness of the proposed method under unobservable conditions, two other indices are selected for the estimation accuracy analysis.

$$\text{Magnitude Error (ME)} = \frac{|V_{\text{se}}-V_{\text{true}}|}{V_{\text{true}}} \tag{28a}$$

$$\text{Phase Angle Error (PAE)} = |\theta_{\text{se}}-\theta_{\text{true}}| \tag{28b}$$

TABLE III

MEASUREMENT CONFIGURATION OF UNOBSERVABLE CONDITION

	Measurement			State	
Type	Number of measurements	Total number of measurements	Number of state variable	Measurement redundancy
AMI	28			
SCADA	18	62	65	0.93
PMU	15			

TABLE IV

SWITCHING PATH OF THE IEEE 33-NODE DISTRIBUTION NETWORK

Order	Closed switch	Open switch	Measurement dispersion	Rank of combined matrix
1	25-29, 8-21, 12-22	23-24, 6-7, 9-10	0.4193	60
2	6-7, 9-10, 23-24	8-21, 2-19, 3-23	0.4140	64
3	18-33, 9-15, 2-19, 3-23	25-29, 12-22, 10-11, 6-26	0.3543	65

Table V lists the state estimation results under the unobservable condition. Owing to insufficient measurement configuration, the traditional Gauss–Newton method is no longer applicable. In contrast, Schemes III, IV, and V can still be implemented. In particular, the accuracy of the proposed method is comparable to that of Scheme IV in terms of the voltage amplitude and is significantly better than that of Scheme IV in terms of the voltage phase angle. Compared with Scheme IV, Scheme III improves the estimation accuracy by 35.6% in MAPE. In Scheme V, the proportion of pseudo measurements is 60%. The pseudo-measurement-based method (Scheme V) exhibits superior accuracy in phase angle compared to the proposed method (Scheme III), but demonstrates slightly lower accuracy in amplitude. Further inference can be made that pseudo measurements have a greater impact on voltage amplitude estimation.

TABLE V

COMPARISON OF ESTIMATION ERRORS UNDER UNOBSERVABLE CONDITION

	ME (%)		PAE (rad)		MAPE
	Average	Maximum	Average	Maximum	
Scheme II	/	/	/	/	/
Scheme III	0.4662	0.9894	0.0029	0.0082	1.4649
Scheme IV	0.4213	0.8262	0.0126	0.0266	2.2749
Scheme V	0.4702	0.9902	0.0025	0.0053	1.5539

The estimation error of the proposed method mainly results from the modeling error in (4). The next main task is to reduce the model error in Holt's two-parameter exponential smoothing method. For the matrix completion method, the inability to integrate multi-source measurements into a single matrix affects the estimation accuracy. Specifically, a relatively small number of D-PMU measurements result in significant errors in the voltage phase angle.

For most distribution systems, especially for the unobservable ones, D-PMU measurements are unavailable. Thus, the proposed method is tested under pure AMI and SCADA measurements. The measurement configuration is based on Fig. 4, with D-PMU measurements removed. The results of state estimation are shown in Table VI.

TABLE VI

COMPARISON OF ESTIMATION ERRORS WITH AMI AND SCADA MEASUREMENTS

	ME (%)		PAE (rad)		MAPE
	Average	Maximum	Average	Maximum	
Scheme II	/	/	/	/	/
Scheme III	1.2963	1.9633	0.0042	0.0091	4.2505
Scheme IV	0.9129	1.6951	0.0198	0.0345	5.7531
Scheme V	1.4287	2.1056	0.0035	0.0068	5.0165

It can be seen that the estimation error has increased compared to Table V. Due to the higher measurement accuracy of D-PMU compared to AMI and SCADA, the estimation error increases in pure AMI and SCADA measurement scenarios, which demonstrates the improvement of D-PMU measurement on estimation accuracy. Besides, the proposed method (Scheme III) still has lower estimation errors compared to the matrix completion method (Scheme IV) and the pseudo measurement method (Scheme V) in MAPE, further verifying the advantages of the proposed method. Especially, the lack of D-PMU measurement leads to larger errors in voltage phase angle.

C. *Analysis of Observable Conditions*

To verify the effectiveness of the proposed method under observable conditions, all load nodes are monitored with AMI measurements, and some nodes and lines are monitored with SCADA and D-PMU measurements. The measurement configurations are listed in Table VII. In this case, the measurement configuration already satisfies the stochastic observability condition according to (6); therefore, the state estimation can be solved directly.

TABLE VII

MEASUREMENT CONFIGURATION OF OBSERVABLE CONDITION

Measurement			State	
Type	Number of measurements	Total number of measurements	Number of state variable	Measurement redundancy
AMI	66			
SCADA	18	101	65	1.53
PMU	17			

Table VIII and Fig. 6 present the state estimation results. Taking subsystem 6 as an example, when the measurement configuration is observable, the proposed method (Scheme III) exhibits an estimation accuracy comparable to that of the traditional Gauss-Newton method (Scheme II) and the pseudo-measurement-based method (Scheme V). The main source of error is the linearized measurement function during the solving process. However, in the proposed method, in addition to the assumption of linearized measurement function, there are also modeling errors in the state transition process (4) and the UKF solving process (20)-(22). Due to the calculation starting from the zero initial state and the small number of topology switches, the model does not closely approach the actual nonlinear model. Besides, the predicted covariance matrix $\boldsymbol{Q}_k$ has a significant impact on the performance of the UKF algorithm. Although the improved fault-tolerant noise statistical estimator (26) is proposed in this paper, the process error cannot be completely eliminated.

TABLE VIII

COMPARISON OF ESTIMATION ERRORS UNDER OBSERVABLE CONDITION

	ME (%)		PAE (rad)		MAPE
	Average	Maximum	Average	Maximum	
Scheme II	0.3221	1.1682	0.0013	0.0027	0.8531
Scheme III	0.4614	1.2465	0.0015	0.0032	0.9635
Scheme IV	1.3220	2.3873	0.0237	3.4116	4.8564
Scheme V	0.5654	1.3020	0.0012	0.0021	0.9783

Scheme II is based on an accurate nonlinear power flow model but is not applicable to Scheme III. The estimation accuracy of the matrix completion method (Scheme IV) is worse than that of Scheme III, especially in the voltage phase angle. Compared to Scheme IV, Scheme III improves estimation accuracy by over 40% in terms of MAPE. The average estimation error of the nodal voltage magnitude in Scheme III is less than 1%, which satisfies the accuracy requirements of practical applications.

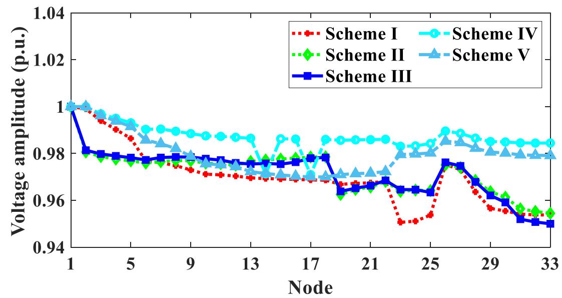

(a) Nodal voltage magnitude of subsystem 6.

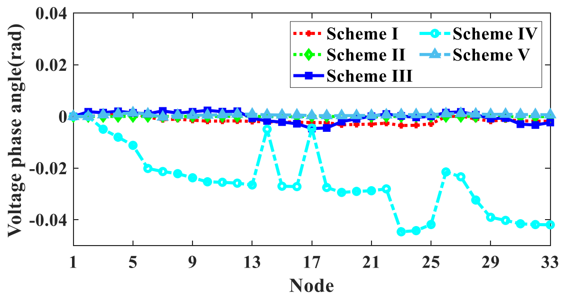

(b) Nodal voltage phase angle of subsystem 6.

Fig. 6. Comparison of state estimation results.

D. *Computational Efficiency Analysis*

Table IX lists the computational times of state estimation with different schemes under different conditions. Note that the computational time in Table IX only includes the calculation time and does not include the time for topology switching.

The matrix completion method in Scheme IV is the most time-consuming because it solves the optimization problem. The computational time increases further in large-scale distribution networks. The proposed method requires only matrix calculations, which significantly reduced the computational burden. Scheme III is more efficient than Scheme IV, doubling the computation speed under unobservable conditions, which effectively ensures real-time performance of state estimation. However, the computational time of Scheme III is more than Scheme V due to the algorithm design. Improving computational efficiency is the focus of our future work.

TABLE IX

COMPUTATIONAL TIME OF THE IEEE 33-NODE DISTRIBUTION NETWORK

	Computational time (s)	
	observable	unobservable
Scheme II	0.0251	/
Scheme III	1.5588	0.8194
Scheme IV	2.7947	1.6750
Scheme V	1.0951	1.1396

E. *Scalability Analysis*

1) Modified IEEE 123-node distribution network

The modified IEEE 123-node distribution network is adopted to verify the scalability of the proposed method. Fig. 7 shows the topology of the test system. Six PVs with capacities of 1000 kWp and three WTs with capacities of 1000 kVA are integrated into the distribution network. The measurement redundancy is 0.89.

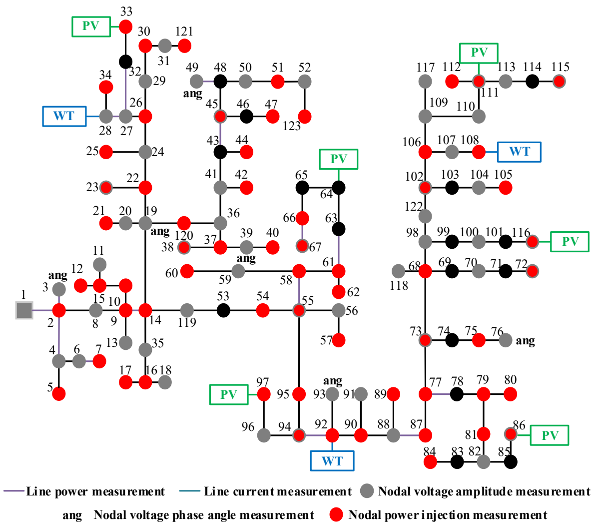

Fig. 7. Structure of modified IEEE 123-node distribution network.

TABLE X

SWITCHING PATH OF THE IEEE 123-NODE DISTRIBUTION NETWORK

Order	Closed switch	Open switch	Measurement dispersion	Rank of combined matrix
1	123-109, 57-73	98-122, 55-95	0.5986	219
2	52-117, 55-95, 98-122, 26-45	123-109, 57-73, 14-19, 41-43	0.4880	231
3	14-19, 41-43, 16-96, 40-67, 19-120	52-117, 98-122, 26-45, 119-53, 19-120	0.4532	245

Due to the unobservable measurement configuration, the switching path is listed in Table X. The state estimation error and computational time are listed in Tables XI. The proposed method has advantages in terms of both the estimation accuracy and computational speed. The computational speed is improved by nearly 20 times, which ensures the real-time performance of the state estimation.

TABLE XI

COMPARISON OF ESTIMATION RESULTS OF THE IEEE 123-NODE DISTRIBUTION NETWORK

	ME (%)		PAE (rad)		MAPE	Computational time (s)
	Average	Maximum	Average	Maximum		
Scheme II	/	/	/	/	/	/
Scheme III	0.3313	0.9494	0.0388	0.1029	1.1649	52.6863
Scheme IV	0.3660	1.0262	0.0766	0.1453	1.8749	1284.5349
Scheme V	0.3522	0.9956	0.0325	0.0780	1.3024	32.8169

2) Practical pilot in Guangzhou, China

A case from a practical pilot in Guangzhou, China is adopted to verify the feasibility of the proposed method. The topology and measurement configuration are shown in Fig. 8. The system consists of 52 lines, with a rated voltage level of 10 kV, and the total active power and reactive power demands are 8790 kW and 1786 kVAr, respectively. It is worth noting that the network structure and parameters are derived from the real practical pilot, and the operational states of sources and loads are derived from simulations. The measurement values generated by simulation and scheme settings are similar to those in Section IV.A.

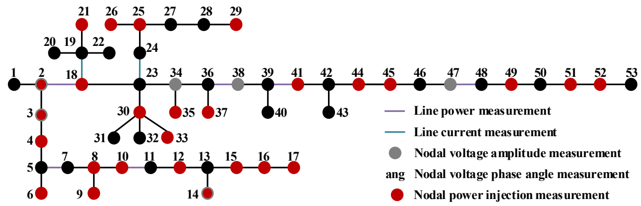

Fig. 8. Structure of the practical pilot in Guangzhou.

TABLE XII
COMPARISON OF ESTIMATION RESULTS OF THE PRACTICAL PILOT IN GUANGZHOU

	ME (%)		PAE (rad)		MAPE	Computational time (s)
	Average	Maximum	Average	Maximum		
Scheme II	/	/	/	/	/	/
Scheme III	0.5419	1.2932	0.0173	0.0340	1.1645	4.9125
Scheme IV	1.3324	1.5328	0.0176	0.0221	2.2512	7.8951
Scheme V	0.7365	1.6874	0.0126	0.0260	1.3688	3.0091

Table XII shows the state estimation results of the practical pilot in Guangzhou. The proposed method still has advantages in terms of both the estimation accuracy and computational speed, which is consistent with previous analysis. Due to the limited D-PMU measurements, the estimation error of the proposed method is slightly lower than the results of the simulation cases, but still meets practical needs.

In summary, the proposed state estimation method for unobservable distribution networks can conduct accurate state estimation under unobservable conditions and has satisfactory computational speed in large-scale systems. Thus, the proposed method is a promising solution for state perception.

V. Conclusions

To realize the accurate and fast state perception of unobservable distribution networks, this paper proposes a state estimation method for unobservable distribution networks based on random state switching. First, the RSADN is modeled, and stochastic observability is defined to cope with unobservable conditions. The switching-guiding mechanism is designed to reduce the frequent switching of the RSADN. Subsequently, the improved UKF algorithm is utilized to solve the state estimation problem based on state transformation. The results show that the proposed method can conduct accurate state estimation under unobservable conditions and has a satisfactory computational speed in large-scale systems.

Future research can be conducted from the following perspectives. First, simplifying the algorithm process and improving code efficiency to further improve efficiency is worth studying. Second, reducing the error of linear model further improves estimation accuracy. Finally, robustness to bad data should be thoroughly investigated in unobservable distribution networks.

References

[1] B. A. Alcaide-Moreno, C. R. Fuerte-Esquivel, M. Glavic and T. Van Cutsem, "Electric power network state tracking from multirate measurements," *IEEE Transactions on Instrumentation and Measurement*, vol. 67, no. 1, pp. 33-44, 2018.

[2] M. Vanin, T. Van Acker, R. D'hulst and D. Van Hertem, "Exact modeling of non-gaussian measurement uncertainty in distribution system state estimation," *IEEE Transactions on Instrumentation and Measurement*, vol. 72, pp. 1-11, 2023, Art no. 9002911.

[3] A. Akrami and H. Mohsenian-Rad, "Event-triggered distribution system state estimation: sparse Kalman filtering with reinforced coupling," *IEEE Transactions on Smart Grid*, vol. 15, no. 1, pp. 627-640, 2024.

[4] J. Zhao, L. Mili and R. C. Pires, "Statistical and numerical robust state estimator for heavily loaded power systems," *IEEE Transactions on Power Systems*, vol. 33, no. 6, pp. 6904-6914, 2018.

[5] Y. Lan, H. Zhu and X. Guan, "Fast nonconvex SDP solvers for large-scale power system state estimation," *IEEE Transactions on Power Systems*, vol. 35, no. 3, pp. 2412-2421, 2020.

[6] Z. Liu et al., "Robust state estimation of active distribution networks with multi-source measurements," *Journal of Modern Power Systems and Clean Energy*, vol. 11, no. 5, pp. 1540-1552, 2023.

[7] T. Chen, H. Ren, E. Y. S. Foo, L. Sun and G. A. J. Amaratunga, "A fast and robust state estimator based on exponential function for power systems," *IEEE Sensors Journal*, vol. 22, no. 6, pp. 5755-5767, 2022.

[8] K. Dehghanpour, Y. Yuan, Z. Wang and F. Bu, "A game-theoretic data-driven approach for pseudo-measurement generation in distribution system state estimation," *IEEE Transactions on Smart Grid*, vol. 10, no. 6, pp. 5942-5951, 2019.

[9] K. R. Mestav, J. Luengo-Rozas and L. Tong, "Bayesian state estimation for unobservable distribution systems via deep learning," *IEEE Transactions on Power Systems*, vol. 34, no. 6, pp. 4910-4920, 2019.

[10] B. Azimian, R. S. Biswas, S. Moshtagh, A. Pal, L. Tong and G. Dasarathy, "State and topology estimation for unobservable distribution systems using deep neural networks," *IEEE Transactions on Instrumentation and Measurement*, vol. 71, pp. 1-14, Art no. 9003514, 2022.

[11] J. Im, J. Ban, Y. -J. Kim and J. Zhao, "PMU-based distributed state estimation to enhance the numerical stability using equality constraints," *IEEE Transactions on Power Systems*, vol. 39, no. 2, pp. 4409-4421, 2024.

[12] A. Mokaribolhassan, G. Nourbakhsh, G. Ledwich, A. Arefi and M. Shafiei, "Distribution system state estimation using PV separation strategy in lv feeders with high levels of unmonitored PV generation," *IEEE Systems Journal*, vol. 17, no. 1, pp. 684-695, 2023.

[13] M. Vanin, T. Van Acker, R. D'hulst and D. V. Hertem, "A framework for constrained static state estimation in unbalanced distribution networks," *IEEE Transactions on Power Systems*, vol. 37, no. 3, pp. 2075-2085, May 2022.

[14] M. Vanin, T. Van Acker, R. D'hulst and D. Van Hertem, "Exact modeling of non-gaussian measurement uncertainty in distribution system state estimation," *IEEE Transactions on Instrumentation and Measurement*, vol. 72, pp. 1-11, 2023, Art no. 9002911.

[15] A. Angioni, T. Schlösser, F. Ponci and A. Monti, "Impact of pseudo-measurements from new power profiles on state estimation in low-voltage grids," *IEEE Transactions on Instrumentation and Measurement*, vol. 65, no. 1, pp. 70-77, 2016.

[16] J. Zhang, J. Zhao, J. Yang and J. Zhao, "Deep multi-fidelity Bayesian data fusion for probabilistic distribution system voltage estimation with high penetration of PVs," *IEEE Transactions on Power Systems*, vol. 39, no. 2, pp. 3661-3672, 2024.

[17] G. Tian, Y. Gu, D. Shi, J. Fu, Z. Yu and Q. Zhou, "Neural-network-based power system state estimation with extended observability," *Journal of Modern Power Systems and Clean Energy*, vol. 9, no. 5, pp. 1043-1053, 2021.

[18] M. Pau and P. A. Pegoraro, "WLS-based state estimation for unobservable distribution grids through allocation factors evaluation," *IEEE Transactions on Instrumentation and Measurement*, vol. 73, pp. 1-13, Art no. 9003013, 2024.

[19] P. L. Donti, Y. Liu, A. J. Schmitt, A. Bernstein, R. Yang and Y. Zhang, "Matrix completion for low-observability voltage estimation," *IEEE Transactions on Smart Grid*, vol. 11, no. 3, pp. 2520-2530, 2020.

[20] B. Rout, S. Dahale and B. Natarajan, "Dynamic matrix completion based state estimation in distribution grids," *IEEE Transactions on Industrial Informatics*, vol. 18, no. 11, pp. 7504-7511, 2022.

[21] L. Y. Wang, G. Yin, F. Lin, M. P. Polis and W. Chen, "Stochastic observability and convergent analog state estimation of randomly switched linear systems with unobservable subsystems," *IEEE Transactions on Automatic Control*, vol. 68, no. 2, pp. 898-911, 2023.

[22] L. Y. Wang, G. Yin, F. Lin, M. P. Polis and W. Chen, "Joint estimation of continuous and discrete states in randomly switched linear systems with unobservable subsystems," *IEEE Transactions on Automatic Control*, vol. 68, no. 10, pp. 6007-6019, 2023.

[23] Kong, X. Zhang, X. Zhang, C. Wang, H. -D. Chiang and P. Li, "Adaptive dynamic state estimation of distribution network based on interacting multiple model," *IEEE Transactions on Sustainable Energy*, vol. 13, no. 2, pp. 643-652, 2022.

[24] D. Xu, Z. Wu, J. Xu, Y. Zhu and Q. Hu, "A multiarea forecasting-aided state estimation strategy for unbalance distribution networks," *IEEE Transactions on Industrial Informatics*, vol. 20, no. 1, pp. 806-814, 2024.

[25] X. Kong, X. Zhang, X. Zhang, C. Wang, H. -D. Chiang and P. Li, "Adaptive dynamic state estimation of distribution network based on interacting multiple model," *IEEE Transactions on Sustainable Energy*, vol. 13, no. 2, pp. 643-652, 2022.

[26] R. C. Dugan, *Reference Guide for the Open Distribution System Simulator (OpenDSS)*, Elect. Power Res. Inst., Palo Alto, CA, USA, 2016.

APPENDIX

A. Proof of Lemma 1

1) From $\boldsymbol{T}_k$, $\boldsymbol{F}_k\boldsymbol{Y}_k = 0$ holds. If $\boldsymbol{\lambda} \in \ker(\boldsymbol{W}_k)$, then $\boldsymbol{\lambda} = \boldsymbol{Y}_k\boldsymbol{\varpi}$ for some $\boldsymbol{\varpi} \in \mathbb{R}^{s-s_k}$. This implies that $\boldsymbol{F}_k\boldsymbol{\lambda} = \boldsymbol{F}_k\boldsymbol{Y}_k\boldsymbol{\varpi} = 0$. Hence, $\boldsymbol{\lambda} \in \ker(\boldsymbol{F}_k)$.

Conversely, if $\boldsymbol{\lambda} \in \ker(\boldsymbol{F}_k)$, then $\boldsymbol{F}_k\boldsymbol{\lambda} = 0$ and the following equation holds:

$$\begin{aligned}\boldsymbol{\lambda} &= \boldsymbol{T}_k\boldsymbol{T}_k^{-1}\boldsymbol{\lambda} = [\boldsymbol{Y}_k, \boldsymbol{Z}_k]\begin{bmatrix}\boldsymbol{G}_k\\ \boldsymbol{F}_k\end{bmatrix}\boldsymbol{\lambda} \\ &= [\boldsymbol{Y}_k, \boldsymbol{Z}_k]\begin{bmatrix}\boldsymbol{G}_k\boldsymbol{\lambda}\\ 0\end{bmatrix} = \boldsymbol{Y}_k\boldsymbol{G}_k\boldsymbol{\lambda}\end{aligned} \tag{A.1}$$

which implies that $\boldsymbol{\lambda} \in \mathrm{Range}(\boldsymbol{Y}_k) = \ker(\boldsymbol{W}_k)$.

2) By defining $\boldsymbol{F}$ and $\boldsymbol{W}_\Theta$, the following equation holds:

$$\ker(\boldsymbol{W}_\Theta) = \cap_{i=1}^{k}\ker(\boldsymbol{W}_i) \tag{A.2}$$

$$\ker(\boldsymbol{F}) = \cap_{i=1}^{k}\ker(\boldsymbol{F}_i) \tag{A.3}$$

As $\ker(\boldsymbol{W}_i) = \ker(\boldsymbol{F}_i)$, the conclusion holds.

B. Operation curves of DGs and loads.

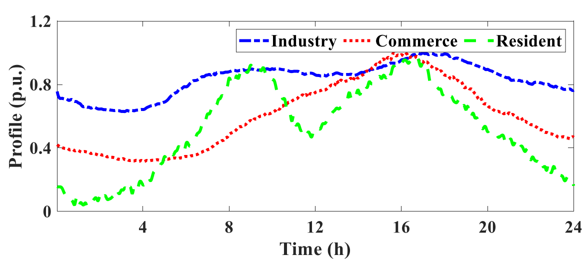

(a) Operation curves of loads.

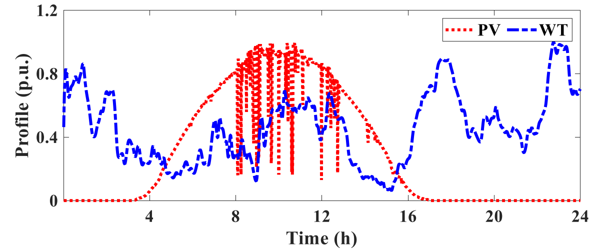

(b) Operation curves of DGs.

Fig. B. Operation curves of DGs and loads.

C. Matrix Completion State Estimation Method

The matrix completion state estimation method can be expressed as the following semi-definite positive optimization problem:

$$\min_{\boldsymbol{X},\boldsymbol{D}_1,\boldsymbol{D}_2} \mathrm{trace}(\boldsymbol{D}_1) + \mathrm{trace}(\boldsymbol{D}_2) + \textstyle\sum_{\epsilon\in\boldsymbol{E}} w_\epsilon||\boldsymbol{\epsilon}|| \tag{A.4}$$

$$\mathrm{s.t.}\ ||\boldsymbol{X}_\Psi - \boldsymbol{M}_\Psi||_F \le \delta \tag{A.5}$$

$$\begin{bmatrix}-\tau_r\\ -\tau_c\end{bmatrix} \le \begin{bmatrix}\Re\left(\boldsymbol{v}_{-1} - \left(\boldsymbol{A}\begin{bmatrix}\Re(\boldsymbol{s}_{-1})\\ \Im(\boldsymbol{s}_{-1})\end{bmatrix} + \boldsymbol{w}\right)\right)\\ \Im\left(\boldsymbol{v}_{-1} - \left(\boldsymbol{A}\begin{bmatrix}\Re(\boldsymbol{s}_{-1})\\ \Im(\boldsymbol{s}_{-1})\end{bmatrix} + \boldsymbol{w}\right)\right)\end{bmatrix} \le \begin{bmatrix}\tau_r\\ \tau_c\end{bmatrix}, \tag{A.6}$$

$$-\boldsymbol{\gamma} \le |\boldsymbol{v}_{-1}| - \left(\boldsymbol{C}\begin{bmatrix}\Re(\boldsymbol{s}_{-1})\\ \Im(\boldsymbol{s}_{-1})\end{bmatrix} + |\boldsymbol{w}|\right) \le \boldsymbol{\gamma} \tag{A.7}$$

$$\begin{bmatrix}-\alpha_r\\ -\alpha_c\end{bmatrix} \le \begin{bmatrix}\Re(\boldsymbol{s}_1 - (\boldsymbol{v}_1(\boldsymbol{Y}_{11}^*\boldsymbol{v}_1^* + \boldsymbol{Y}_{1L}^*\boldsymbol{v}_{-1}^*)))\\ \Im(\boldsymbol{s}_1 - (\boldsymbol{v}_1(\boldsymbol{Y}_{11}^*\boldsymbol{v}_1^* + \boldsymbol{Y}_{1L}^*\boldsymbol{v}_{-1}^*)))\end{bmatrix} \le \begin{bmatrix}\alpha_r\\ \alpha_c\end{bmatrix} \tag{A.8}$$

$$\boldsymbol{\epsilon} \ge \boldsymbol{0}, \forall\boldsymbol{\epsilon} \in \boldsymbol{E} \tag{A.9}$$

$$\begin{bmatrix}\boldsymbol{D}_1 & \boldsymbol{X}\\ \boldsymbol{X}^{\mathrm{T}} & \boldsymbol{D}_2\end{bmatrix} \succcurlyeq 0 \tag{A.10}$$

In this paper, $\delta = 0.01$. This problem can be solved directly using a semi-definite positive optimizer (e.g., SeDuMi).

D. Calculation process of the combined matrix

The observability matrix $\boldsymbol{W}_1$ of topology 1 is shown as follows.

$W_1=$

	1	2	3	4	5	6	7		1	2	3	4	5	6	7
1	-1379	1971	-258	-334	-703	1004	-131	25	-1379	1970	-258	-333	-703	1004	-131
2	-703	1004	-131	-170	1379	-1971	257	26	-703	1004	-131	-169	1379	-1970	257
3	0	1380	-1379	0	0	702	-702	27	0	1379	-1379	0	0	702	-702
4	0	703	-703	0	0	-1387	1387	28	0	703	-703	0	0	-1378	1378
5	0	1538	0	-1538	0	-180	0	29	0	1538	0	-1538	0	-180	0
6	1	0	0	0	0	0	0	30	1	0	0	0	0	0	0
7	-1379	1971	-258	-333	-703	1044	-131	31	-1379	1970	-258	-333	-703	1004	-131
8	-703	1004	-131	-170	1379	-1970	257	32	-703	1004	-131	-169	1379	-1970	257
9	0	1379	-1379	0	0	702	-702	33	0	1379	-1379	0	0	702	-702
10	0	703	-703	0	0	-1378	1378	34	0	703	-703	0	0	-1378	1378
11	0	1538	0	-1538	0	-180	0	35	0	1538	0	-1538	0	-180	0
12	1	0	0	0	0	0	0	36	1	0	0	0	0	0	0
13	-1379	1970	-258	-333	-703	1004	-131	37	-1379	1970	-258	-333	-703	1004	-131
14	-703	1004	-131	-169	1379	-1970	257	38	-703	1004	-131	-169	1379	-1970	257
15	0	1379	-1379	0	0	702	-702	39	0	1379	-1379	0	0	702	-702
16	0	703	-703	0	0	-1378	1378	40	0	703	-703	0	0	-1378	1378
17	0	1538	0	-1538	0	-180	0	41	0	1538	0	-1538	0	-180	0
18	1	0	0	0	0	0	0	42	1	0	0	0	0	0	0
19	-1379	1970	-258	-333	-703	1004	-131	43	-1379	1970	-258	-333	-703	1004	-131
20	-703	1004	-131	-169	1379	-1970	257	44	-703	1004	-131	-169	1379	-1970	257
21	0	1379	-1379	0	0	702	-702	45	0	1379	-1379	0	0	702	-702
22	0	703	-703	0	0	-1378	1378	46	0	703	-703	0	0	-1378	1378
23	0	1538	0	-1538	0	-180	0	47	0	1538	0	-1538	0	-180	0
24	1	0	0	0	0	0	0	48	1	0	0	0	0	0	0

$\mathrm{rank}(W_1) = 6$

The topology 4 is selected as the switching path, so the combined matrix $\boldsymbol{W}_\Theta$ is shown as follows.

$W_{\Theta} =$

	1	2	3	4	5	6	7		1	2	3	4	5	6	7
1	-1379	1971	-258	-334	-703	1004	-131	41	0	1538	0	-1538	0	-180	0
2	-703	1004	-131	-170	1379	-1971	257	42	1	0	0	0	0	0	0
3	0	1380	-1379	0	0	702	-702	43	-1379	1970	-258	-333	-703	1004	-131
4	0	703	-703	0	0	-1387	1387	44	-703	1004	-131	-169	1379	-1970	257
5	0	1538	0	-1538	0	-180	0	45	0	1379	-1379	0	0	702	-702
6	1	0	0	0	0	0	0	46	0	703	-703	0	0	-1378	1378
7	-1379	1971	-258	-333	-703	1044	-131	47	0	1538	0	-1538	0	-180	0
8	-703	1004	-131	-170	1379	-1970	257	48	1	0	0	0	0	0	0
9	0	1379	-1379	0	0	702	-702	49	-1379	1713	0	-333	-703	873	0
10	0	703	-703	0	0	-1378	1378	50	-703	873	0	-170	1379	-1713	0
11	0	1538	0	-1538	0	-180	0	51	0	1538	0	-1538	0	-180	0
12	1	0	0	0	0	0	0	52	1	0	0	0	0	0	0
13	-1379	1970	-258	-333	-703	1004	-131	53	-1379	1713	0	-333	-703	873	0
14	-703	1004	-131	-169	1379	-1970	257	54	-703	873	0	-170	1379	-1713	0
15	0	1379	-1379	0	0	702	-702	55	0	1538	0	-1538	0	-180	0
16	0	703	-703	0	0	-1378	1378	56	1	0	0	0	0	0	0
17	0	1538	0	-1538	0	-180	0	57	-1379	1713	0	-333	-703	873	0
18	1	0	0	0	0	0	0	58	-703	873	0	-170	1379	-1713	0
19	-1379	1970	-258	-333	-703	1004	-131	59	0	1538	0	-1538	0	-180	0
20	-703	1004	-131	-169	1379	-1970	257	60	1	0	0	0	0	0	0
21	0	1379	-1379	0	0	702	-702	61	-1379	1713	0	-333	-703	873	0
22	0	703	-703	0	0	-1378	1378	62	-703	873	0	-170	1379	-1713	0
23	0	1538	0	-1538	0	-180	0	63	0	1538	0	-1538	0	-180	0
24	1	0	0	0	0	0	0	64	1	0	0	0	0	0	0
25	-1379	1970	-258	-333	-703	1004	-131	65	-1379	1713	0	-333	-703	873	0
26	-703	1004	-131	-169	1379	-1970	257	66	-703	873	0	-170	1379	-1713	0
27	0	1379	-1379	0	0	702	-702	67	0	1538	0	-1538	0	-180	0
28	0	703	-703	0	0	-1378	1378	68	1	0	0	0	0	0	0
29	0	1538	0	-1538	0	-180	0	69	-1379	1713	0	-333	-703	873	0
30	1	0	0	0	0	0	0	70	-703	873	0	-170	1379	-1713	0
31	-1379	1970	-258	-333	-703	1004	-131	71	0	1538	0	-1538	0	-180	0
32	-703	1004	-131	-169	1379	-1970	257	72	1	0	0	0	0	0	0
33	0	1379	-1379	0	0	702	-702	73	-1379	1713	0	-333	-703	873	0
34	0	703	-703	0	0	-1378	1378	74	-703	873	0	-170	1379	-1713	0
35	0	1538	0	-1538	0	-180	0	75	0	1538	0	-1538	0	-180	0
36	1	0	0	0	0	0	0	76	1	0	0	0	0	0	0
37	-1379	1970	-258	-333	-703	1004	-131	77	-1379	1713	0	-333	-703	873	0
38	-703	1004	-131	-169	1379	-1970	257	78	-703	873	0	-170	1379	-1713	0
39	0	1379	-1379	0	0	702	-702	79	0	1538	0	-1538	0	-180	0
40	0	703	-703	0	0	-1378	1378	80	1	0	0	0	0	0	0

$\mathrm{rank}(W_{\Theta}) = 7$